Applied Catalysis A: General 468 (2013) 44–51

Contents lists available at ScienceDirect

Applied Catalysis A: General

journal homepage: www.elsevier.com/locate/apcata

An efficient Ni–Mo–K sulfide catalyst doped with CNTs for conversion of syngas to ethanol and higher alcohols

Ji-Jie Wang, Jian-Rong Xie, Yan-Hui Huang, Bing-Hui Chen, Guo-Dong Lin, Hong-Bin Zhang*

College of Chemistry and Chemical Engineering, State Key Laboratory of Physical Chemistry for Solid Surfaces and National Engineering Laboratory for Green Chemical Productions of Alcohols–Ethers–Esters, Xiamen University, Xiamen 361005, China

ARTICLE INFO

Article history:
Received 11 June 2013
Received in revised form 8 August 2013
Accepted 15 August 2013
Available online 26 August 2013

Keywords:
Multiwalled carbon nanotubes
CNT-doped Ni–Mo–K sulfide catalyst
Higher alcohol synthesis
Ethanol synthesis
Syngas

ABSTRACT

A type of Ni–Mo–K sulfide catalyst doped with CNTs for conversion of syngas to ethanol and higher alcohols was developed, and displayed high activity and selectivity for direct synthesis of C_{1-4}-alcohols, especially ethanol, from syngas. Over a $Ni_{0.5}Mo_1K_{0.5}$–15%CNTs catalyst under the reaction conditions of 8.0 MPa and 593 K, the *S*(total oxy.) reached 64.1% (CO_2-free), with the corresponding *STY*(total oxy.) being 113 mg h^{-1} g^{-1}. Ethanol was the dominant product, with *S*(EtOH) and *STY*(EtOH) reaching 33.1% (CO_2-free) and 55.6 mg h^{-1} g^{-1}, respectively. This *STY*(EtOH)-value was 1.47 times that (37.9 mg h^{-1} g^{-1}) of the CNTs-free counterpart under the same reaction conditions. Addition of a minor amount of CNTs to the sulfurized $Ni_{0.5}Mo_1K_{0.5}$ catalyst caused little change in the E_a for the hydrogenation–conversion of syngas. Appropriately reducing CNT's grain-size could improve its capability to adsorb hydrogen, thus increasing CO hydrogenation–conversion, yet did not influence selectivity of the products. The present work demonstrated that CNTs as promoter function through their adsorbing/activating H_2 to generate a surface micro-environment with higher stationary-state concentration of H-adspecies on the functioning catalyst. This resulted in a dramatic increase, at the surface of the functioning catalyst, of the molar percentage of catalytically active Mo^{4+}/Mo^{5+} species in the total amounts of surface Mo. On the other hand, those active H-species adsorbed at the CNTs surface could be readily transferred to $Ni_iMo_jK_k$ active sites via the CNT-assisted hydrogen spillover. The aforementioned two factors both were conducive to increasing the rate of hydrogenation conversion of syngas.

1. Introduction

Ethanol is being considered as a potential alternative synthetic fuel or fuel-additive for use in automobiles, and as a potential hydrogen source for fuel cells. Renewable ethanol can also serve as a feedstock for the synthesis of a variety of industrial chemicals and polymers. Ethanol can be produced from biomass or coal, and, recently, a worldwide interest in the synthesis of ethanol from biomass- and coal-derived syngas is growing. Significant improvements in catalyst design need to be achieved to make this conversion commercially attractive [1].

The direct conversion of syngas to ethanol and other C_2-oxygenates has been reported by Union Carbide Company as early as 1975 over SiO_2-supported Rh catalyst promoted by metal ions, such as Fe, Mo, Mn, W, Th, and U, in a stirred autoclave reactor [2–5]. The best results were obtained over a catalyst containing 2.5 wt% Rh supported on SiO_2 and promoted by 0.05 wt% Fe. At 573 K and 1030 psi using H_2/CO, the catalyst produced 49% methane, 2.8% methanol, 31.4% ethanol, and 9.1% acetic acid. However, the rates of methanol and ethanol production were about 50 g/($L_{-cat.}$ h). Following this early work, there are several reports on the conversion of syngas to ethanol and other C_{2+}-oxygenates using a wide range of noble metals-based catalysts containing Rh, Ru, and Re supported on various oxides, such as SiO_2, Al_2O_3, CeO_2, ZrO_2 and MgO [3–5]. Although Rh-based catalysts show promise, the commercial viability of these catalysts is questionable due to its availability.

Development of non-noble metals-based catalysts industrially viable for direct synthesis of ethanol and higher alcohols from syngas has been the other focus of R&D efforts. The catalysts reported in previous literatures include mainly modified methanol synthesis catalysts, modified Fischer–Tropsch synthesis catalysts, and MoS_2-based catalysts [6–16]. Most of those catalysts have been extensively studied for the synthesis of mixed higher alcohols containing a small amount of ethanol from syngas, and yet few of them are suitable for the hydrogenation-conversion of syngas with

* Corresponding author. Tel.: +86 592 2181888; fax: +86 592 2181888.
E-mail addresses: wangjijie1985@xmu.edu.cn (J.-J. Wang), jianronx@xmu.edu.cn (J.-R. Xie), yhhuang@xmu.edu.cn (Y.-H. Huang), chenbh@xmu.edu.cn (B.-H. Chen), gdlin@xmu.edu.cn (G.-D. Lin), hbzhang@xmu.edu.cn (H.-B. Zhang).

0926-860X/$ – see front matter © 2013 Elsevier B.V. All rights reserved.
http://dx.doi.org/10.1016/j.apcata.2013.08.026

ethanol as the major product. Recently, there are several reports on new catalyst systems, such as K_2CO_3/Co–MoS_2/clay catalyst [12], K and Ni doped β-Mo_2C catalyst [13], and Al_2O_3 (or AC)-suppoted Ni(or Co, Rh)-promoted, K-modified MoS_2 catalysts [16], over which the selectivity to form ethanol and higher alcohols from hydrogenation–conversion of syngas has improved markedly to different extent. Nevertheless, from the practical viewpoint, the selectivity and yield of desired alcohol products of those catalysts still need to be further improved.

Multi-walled carbon-nanotubes (donated as "CNTs" in later text) have been drawing increasing attention in recent years. This kind of nanotube-C material possesses a series of unique features, such as its highly conductive graphitized tube-wall, nanometer-sized channel and sp^2-C-constructed surface, as well as excellent performance for adsorption and spillover of hydrogen, which make CNTs full of promise to be a novel catalyst support or promoter. The catalytic studies conducted so far on CNT-based systems have shown encouraging results in terms of activity and selectivity [17–19].

In the present work, a type of co-precipitated–deposited Ni–Mo–K sulfide-based catalyst doped with CNTs was developed. The catalyst displayed higher activity and selectivity for direct synthesis of ethanol and higher alcohols from syngas, compared to the CNT-free host catalyst. The catalyst was characterized by means of TEM, XRD, XPS, H_2S/H_2-TPS and H_2-TPD, and the nature of the promoter action by CNTs was discussed. The results shed light on the design of practical catalysts for direct synthesis of ethanol and higher alcohols from syngas.

2. Experimental

2.1. Catalyst preparation

The CNTs used in the present work were prepared according to the methods reported previously [20]. Freshly prepared CNTs were treated with boiling nitric acid (8 mol/L, at 363 K) for 8 h, followed by rinsing with de-ionized water twice, and then drying at 383 K under N_2-atmosphere. Open-end CNTs with hydrophilic surface were then obtained (see Fig. S1). The dried CNTs were crushed, and sieved to a grain-size of ≤75 μm for the catalyst preparation.

A series of CNT-doped Ni–Mo–K catalysts, denoted as $Ni_iMo_jK_k$–*x*%CNTs (where *x*% represented mass percentage), were prepared by combined co-precipitation and impregnation method. Two aqueous solutions containing calculated amounts of $Ni(NO_3)_2{\cdot}6H_2O$ and $(NH_4)_6Mo_7O_{24}{\cdot}4H_2O$ (all of AR grade), respectively, were simultaneously added dropwise under ultrasonic agitation into a Pyrex flask containing a calculated amount of CNTs at 353 K. After 30 min of ultrasonic agitation, an appropriate amount of ammonia liquor was added into the aforementioned solution to adjust and maintain the pH value of the solution at ~7 so as to form precipitate. The suspension was continuously stirred for 2 h at 353 K, followed by cooling down to room temperature, aging for 4 h before filtering. The filter cake (precipitate) was dried at 383 K for 4 h and calcined at 823 K in N_2 atmosphere for 4 h, followed by cooling down to room temperature. They were next impregnated with K_2CO_3 aqueous solution containing a calculated amount of K by the conventional incipient wetness method, followed by aging for 10 h, drying at 383 K for 4 h and calcining at 673 K under N_2 atmosphere for 4 h, finally yielding the precursor of CNT-doped Ni–Mo–K catalysts (in oxidation state). A CNT-free oxide precursor of Ni–Mo–K catalyst (denoted as $Ni_iMo_jK_k$), used as reference, was prepared in the similar manner. All samples of catalyst precursor were pressed, crushed, and sieved to a size of 40–80 mesh for the activity evaluation.

2.2. Catalyst evaluation

Activity tests of the catalysts for conversion of syngas to ethanol and higher alcohols were carried out in a fixed-bed continuous-flow reactor-GC combination system. Catalyst (1.0 g) was mixed with 4.0 g quartz sand (inert diluents, 40–80 mesh) in order to maintain isothermal conditions, and placed in the reactor. Prior to the reaction, the sample of oxide-precursor of catalyst was in situ pre-reduced/sulfurized in a H_2-carried 5% CS_2 gaseous mixture stream at 0.2 MPa and 1800 mL h^{-1} g^{-1}. The sulfurization temperature was programmed to rise from room temperature to 673 K and maintain at 673 K for 6 h, and then lower to desired temperature for the catalyst test. The hydrogenation–conversion reaction of syngas was conducted at a stationary state under reaction conditions of 5.0–8.0 MPa, 573–623 K, $V(H_2)/V(CO)/V(N_2)$ = 45/45/10 and *GHSV* = 3000–6000 mL h^{-1} g^{-1}. Exit gas from the reactor was immediately transported, while maintaining at 473 K, to the sampling valve of the GC (Model GC-950 by Shanghai Haixin GC Instruments, Inc.), which was equipped with dual detectors (TCD and FID) and dual columns filled with carbon molecular sieve (TDX-201, Tianjin Chem. Reagent Co. Ltd.) and capillary column (TG-BONDQ, USA), respectively, for online analysis. The former column (2.0 m length) was used for the analysis of N_2 (as an internal standard), CO and CO_2, and the latter (30 m × 0.32 mm × 10 μm) for hydrocarbons, alcohols, and other C-containing hydrogenation products. CO conversion (denoted as *X*(CO)) was determined through an internal standard (N_2), and the carbon-based selectivity for the carbon-containing products, including alcohols, hydrocarbons (HC), and other oxygenates (noted as $S_{alc.}$, S_{HC}, etc. in later text), was calculated by an internal normalization method. The description about calculation procedure of space–time–yield (*STY*) of the products is lengthy and was placed in the Supplementary materials. All data were taken 24 h after the reaction started (unless otherwise specified).

2.3. Catalyst characterization

TEM measurements were performed on Technai F30 or JEM-1400 transmission electron microscope. XRD measurements were carried out on an X'Pert PRO X-ray diffractometer (PANalytical) with Cu Kα ($\lambda_{\alpha1}$ = 0.15406 nm, $\lambda_{\alpha2}$ = 0.15443 nm) radiation operating at 40 kV and 30 mA. A continuous scan mode was used to collect 2θ data from 10° to 90°. X-ray photoelectron spectroscopy (XPS) measurements were done on a Quantum 2000 Scanning ESCA Microprobe instrument with Al Kα radiation (15 kV, 25 W, $h\nu$ = 1486.6 eV) under ultrahigh vacuum (5×10^{-7} Pa), calibrated internally by the carbon deposit C(1*s*) (E_b = 284.7 eV). Specific surface area (SSA) was determined by N_2 adsorption using a Micromeritics ASAP 2020 system.

Tests of temperature-programmed reduction/sulfurization by H_2S/H_2 (labeled as H_2S/H_2-TPS) of the catalysts in oxidation state were conducted on a fixed-bed continuous-flow micro-reactor. An anhydrous $CaCl_2$-column and a 3A-zeolite column were installed in sequence at the reactor-exit to remove water vapor yielded from reduction and sulfurization of metal oxides of the catalyst sample. Fifty mg of catalyst sample (in size of 40–80 mesh) in oxidation state was used for each test. The sample was first flushed by an Ar (of 99.999% purity) stream (30 mL min^{-1}) at 573 K for 60 min to clean its surface, and then cooled down to room temperature, followed by switching to a H_2-carried 10 vol% H_2S gaseous mixture as reducing/sulfurizing gas (30 mL min^{-1}) to start the TPS measurement from 298 K to 1073 K. The rate of temperature increase was

10 K min^{-1}. Change of H_2S-signal was monitored by an on-line GC (Shimadzu GC-8A) with a TCD detector.

Tests of H_2-temperature-programmed desorption (H_2-TPD) of the catalysts were conducted on an adsorption/desorption system. Two hundreds mg of sample of the pre-reduced/sulfurized catalyst was used in each test. Prior to the H_2-TPD test, the sample of the pre-reduced/sulfurized catalyst was in situ treated in a H_2 (of 99.999% purity) stream (1800 mL h^{-1}) at 673 K for 3 h and then flushed by an Ar (of 99.999% purity) stream (1800 mL h^{-1}) at 673 K for 60 min to clean its surface, and then cooled down to 433 K, followed by switching to the H_2 (of 99.999% purity) stream for hydrogen adsorption for 60 min and subsequently at room temperature for 2 h. Afterwards, the sample was flushed by the Ar stream at room temperature until the stable baseline in GC appeared. TPD measurements were then conducted from 298 K to 923 K. The rate of temperature increase was 5 K min^{-1}. Change of hydrogen-signal was monitored by an on-line GC (Shimadzu GC-8A) with a TCD detector.

3. Results and discussion

3.1. Optimization of the catalyst composition

Reactivity of conversion of syngas to C_{1-4}-alcohols over a series of the sulfurized $Ni_{0.5}Mo_1K_{0.5}$–*x*%CNTs catalysts with varied CNT-doping amount was first investigated. The results (see Fig. 1) showed that the observed carbon-containing products involved oxygenates (simplified as oxy., including $C_{1\sim4}$-alc. and dimethy ether (DME)) and hydrocarbons (simplified as HC, including C_{1-3}-alkanes), as well as CO_2 yielding from the water–gas–shift (WGS) side-reaction. The catalyst with 15% CNT-doping displayed the best catalytic performance among those tested. Over this catalyst under the reaction conditions of 5.0 MPa and 593 K, the hydrogenation–conversion of CO (denoted as *X*(CO-hydr.)) and *S*(total oxy., CO_2-free) reached 8.4% and 67.2%, respectively. The corresponding *Y*(total oxy.) (i.e., yield of the total oxy., defined as the product of *X*(CO-hydr.) and *S*(total oxy., CO_2-free)), reached 5.65%. Ethanol was the major hydrogenation product, with the *S*(EtOH, CO_2-free) and *Y*(EtOH) being 36.1% and 3.03%, respectively.

Next, the Ni/Mo molar ratio (*i*/1) of the $Ni_iMo_1K_{0.5}$–15%CNTs catalysts was optimized. The results showed that, over the catalyst with *i*/1 = 0.5/1 under the aforementioned reaction conditions, the observed *X*(CO-hydr.) was 8.4%, with the corresponding *S*(total oxy., CO_2-free), *S*(EtOH, CO_2-free) and *Y*(EtOH) being 67.2%, 36.1% and 3.03%, respectively. *X*(CO-hydr.) of the other four catalysts with *i*/1 = 0.25, 0.33, 0.75 and 1.0 was 7.7%, 8.0%, 6.6%, 5.3%, successively, with the corresponding *S*(total oxy., CO_2-free) being 64.0%, 64.4%, 72.0%, 74.5%, and the *S*(EtOH, CO_2-free) being 29.0%, 31.2%, 35.0%, 30.8%, and the *Y*(EtOH) being 2.23%, 2.50%, 2.31%, 1.63%, successively. The Ni/Mo molar ratio of 0.5/1 was chosen to be the optimal one (see Fig. S2).

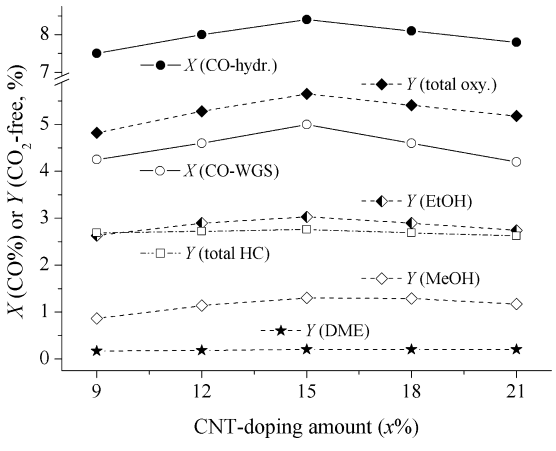

Fig. 1. Reactivity of syngas conversion to ethanol and higher alcohols over the sulfurized $Ni_{0.5}Mo_1K_{0.5}$–*x*%CNTs catalysts with varying CNT-doping amounts, at reaction conditions of 5.0 MPa, 593 K, $V(H_2)/V(CO)/V(N_2)$ = 45/45/10, *GHSV* = 3000 mL h^{-1} g^{-1} (outlet).

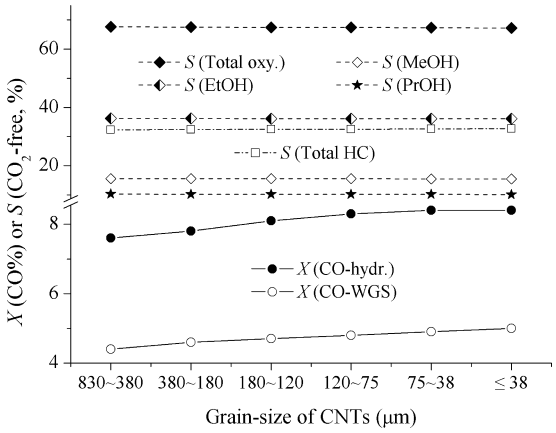

Fig. 2. Reactivity of syngas conversion to ethanol and higher alcohols over the sulfurized $Ni_{0.5}Mo_1K_{0.5}$–15%CNTs catalysts with the CNTs of varying grain-sizes; reaction conditions were the same as in Fig. 1.

Finally, the K/Mo molar ratio (*k*/1) of the $Ni_{0.5}Mo_1K_k$–15%CNTs catalysts was optimized. The results showed that, over the catalyst with *k*/1 = 0.5/1 under the aforementioned reaction conditions, the observed *X*(CO-hydr.) was 8.4%, with the corresponding *S*(total oxy., CO_2-free), *S*(EtOH, CO_2-free) and *Y*(EtOH) being 67.2%, 36.1% and 3.03%, respectively. *X*(CO-hydr.) of the other four catalysts with *k*/1 = 0.3, 0.4, 0.6 and 0.7 was 5.7%, 7.0%, 7.5% and 5.6%, with the corresponding *S*(total oxy., CO_2-free) being 69.9%, 69.5%, 64.5%, 59.3%, and the *S*(EtOH, CO_2-free) being 29.8%, 33.7%, 33.0%, 29.0%, and the *Y*(EtOH) being 1.70%, 2.36%, 2.48%, 1.62%, successively. The K/Mo molar ratio of 0.5/1 was chosen to be the optimal one (see Fig. S3).

Besides the catalyst composition, the grain-size of the used CNTs also has a certain effect on the activity of the corresponding catalyst. Fig. 2 shows the reactivity of syngas conversion to C_{1-4}-alcohols over a series of the sulfurized $Ni_{0.5}Mo_1K_{0.5}$–15%CNTs catalysts with the CNTs of varying grain-sizes. With the grain-size of the CNTs decreasing progressively from the range of 830–380 μm, *X*(CO-hydr.) and *X*(CO-WGS) both increased monotonously before approaching a plateau at 75–38 μm and below. Meanwhile, the *S*(total oxy.), *S*(MeOH), *S*(EtOH) and *S*(PrOH), as well as *S*(total HC), all maintained stable at a respective level. Thus, in order to achieve high conversion of CO hydrogenation, the CNTs with the grain-sizes of ≤75 μm was selected.

3.2. Optimization of the reaction operation conditions

3.2.1. Reaction temperature

Reaction temperature has a pronounced effect on the syngas conversion and the selectivity of the formation of ethanol and higher alcohols. Fig. 3 displays the reactivity of syngas conversion to ethanol and higher alcohols over the sulfurized $Ni_{0.5}Mo_1K_{0.5}$–15%CNTs catalyst at varied temperatures. With the reaction temperature rising progressively from 583 K, *X*(CO-hydr.), *X*(CO-WGS) and *Y*(total HC) increased monotonously; *Y*(ethanol) and *Y*(total oxy.) increased quickly before reaching a maximum at 593 K, and then slowly decreased; while *Y*(MeOH) and *Y*(DME) decreased monotonously. In order to achieve both high *Y*(ethanol) and *Y*(total oxy.), 593 K was taken as the optimal operating temperature.

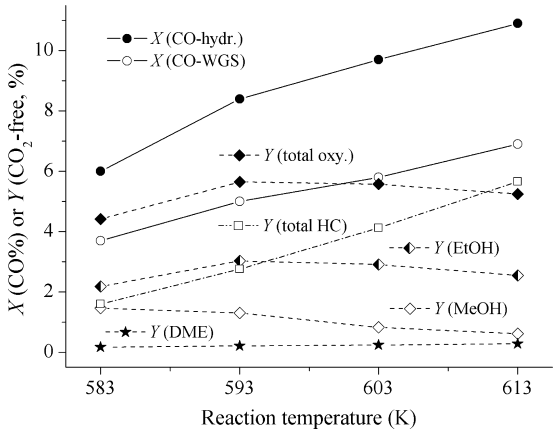

Fig. 3. Reactivity of syngas conversion to ethanol and higher alcohols over the sulfurized $Ni_{0.5}Mo_1K_{0.5}$–15%CNTs catalyst at varied temperatures; reaction conditions were the same as in Fig. 1 except *T* ranging in 573–623 K.

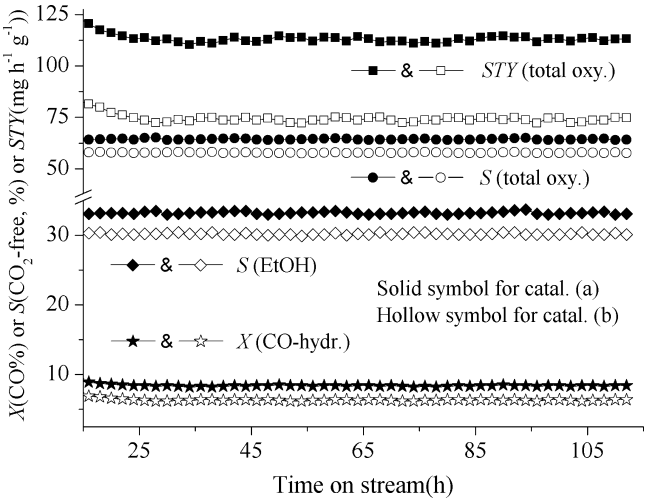

Fig. 4. Operating stability of syngas conversion to ethanol and higher alcohols over the sulfurized $Ni_{0.5}Mo_1K_{0.5}$–15%CNTs catalyst, at reaction conditions of 8.0 MPa, 593 K, $V(H_2)/V(CO)/V(N_2)$ = 45/45/10, *GHSV* = 4000 mL h^{-1} g^{-1} (outlet).

3.2.2. Feed-gas GHSV

In order to find out the working conditions with great extent of reaction, the reaction of syngas converted to ethanol and higher alcohols was conducted over the $Ni_{0.5}Mo_1K_{0.5}$–15%CNTs catalyst under reaction conditions of 8.0 MPa, 593 K, $V(H_2)/V(CO)/V(N_2)$ = 45/45/10 and varied *GHSV* of the feed-gas. The results showed that, with the *GHSV* rising progressively from 3000 to 6000 mL h^{-1} g^{-1}, *X*(CO-hydr.) and *X*(CO-WGS) both decreased monotonously, and *S*(total oxy.) increased slowly but *S*(EtOH) decreased slightly (going down to 31.8% from 34.0%). Meanwhile, *STY*(total oxy.) increased slightly before reaching a maximum at *GHSV* = 4000 mL h^{-1} g^{-1}, and then slowly decreased (see Fig. S4). In order to simultaneously achieve relatively high *X*(CO-hydr.) and *S*(EtOH), as well as *STY*(total oxy.), *GHSV* of the feed-gas was set at 4000 mL h^{-1} g^{-1} (outlet).

3.3. Performance of Ni–Mo–K sulfide catalyst doped with CNTs and reference system

The reaction of syngas converted to ethanol and higher alcohols was conducted under the aforementioned optimized reaction conditions: 8.0 MPa, 593 K, $V(H_2)/V(CO)/V(N_2)$ = 45/45/10 and *GHSV* = 4000 mL h^{-1} g^{-1} (outlet). Table 1 lists the results taken at 100 h after the reaction started. Over the $Ni_{0.5}Mo_1K_{0.5}$–15%CNTs catalyst, *X*(CO-hydr.) reached 8.4%, with the corresponding *STY*(total oxy.) and *STY*(EtOH) being 113 and 55.6 mg h^{-1} g^{-1}, respectively. The two values was 1.51 and 1.47 times those (74.7 and 37.9 mg h^{-1} g^{-1}) of the CNT-free counterpart $Ni_{0.5}Mo_1K_{0.5}$, respectively.

Fig. 4 shows the operation stability of the $Ni_{0.5}Mo_1K_{0.5}$-15%CNTs catalyst and the CNT-free counterpart $Ni_{0.5}Mo_1K_{0.5}$ for the syngas conversion to ethanol and higher alcohols lasting 112 h. Over the $Ni_{0.5}Mo_1K_{0.5}$–15%CNTs catalysts, throughout the reaction, *X*(CO-hydr.), *S*(total oxy.), *S*(EtOH) and *STY*(total oxy.) maintained stable at the level of ~8.4%, ~64%, ~33% and 113 mg h^{-1} g^{-1}, respectively, with no obvious deactivation observed.

The apparent activation energy (E_a) of the hydrogenation-reaction of CO over the two catalysts tested was measured under the reaction conditions of 5.0 MPa, $V(H_2)/V(CO)/V(N_2)$ = 45/45/10, *GHSV* = 6000 mL h^{-1} g^{-1} (outlet), under which the mass transfer limitation was ruled out. The E_a of hydrogenation-reaction of CO observed on the two catalysts, $Ni_{0.5}Mo_1K_{0.5}$–15%CNTs and $Ni_{0.5}Mo_1K_{0.5}$, was 58.6 and 62.1 kJ mol^{-1}, respectively (see Fig. S5). These E_a values were fairly close to each other, indicating that appropriate incorporation of a minor amount of CNTs into the $Ni_{0.5}Mo_1K_{0.5}$ sulfide host catalyst did not cause a marked change in the E_a for the hydrogenation-reaction of CO, most likely implying that such doping did not alter the major reaction pathway of CO hydrogenation.

3.4. Characterization of the catalysts

3.4.1. TEM characterization

Our previous studies [20–22] have demonstrated that this type of CNTs used in the present work was a "Herringbone-type" of multi-walled nanotubes, with the outer diameters of 10–60 nm and the inner diameters of 3–8 nm (see Fig. S1(a)). The content of elemental carbon and graphitized carbon was >99% and ≥90% (mass%), respectively, in the purified CNTs, with the N_2-BET specific surface area (SSA) being ca. 125 m^2 g^{-1} before crushing and sieving. Test of H_2-temperature-programmed hydrogenation (TPH) showed that the temperature needed for initiating the hydrogenation reaction of the CNTs with H_2 was ≥773 K (see Fig. S1(b)), indicating that this type of CNTs was stable in H_2-atmosphere at the reaction temperatures for the hydrogenation-conversion of syngas to ethanol and higher alcohols.

Fig. 5(a) shows the TEM image of the pre-reduced/sulfurized $Ni_{0.5}Mo_1K_{0.5}$–15%CNTs catalyst. The observed the Ni–Mo sulfide nanoparticles were fairly uniform in size and well dispersed on the CNTs or their scraps. Fig. 5 (b) and (c) show the TEM images of the two catalysts, $Ni_{0.5}Mo_1K_{0.5}$–15%CNTs and the CNT-free counterpart, $Ni_{0.5}Mo_1K_{0.5}$, after testing for conversion of syngas to ethanol and higher alcohols under the aforementioned reaction conditions of 8.0 MPa and 593 K for 24 h. Comparatively, the particle sizes of Ni–Mo–K sulfide species were significantly smaller in the CNT-containing catalyst than those in CNT-free counterpart (Fig. 5 (b) vs. (c)).

3.4.2. XRD characterization of the catalysts

The XRD post-reaction analysis (see Fig. 6) showed that there were few differences between the two used catalysts in their XRD features related with the Ni–Mo–K components, except the feature at $2\theta = 26.1^\circ$ for the CNT-containing system (see Fig. 6(a)), which was due to the diffraction of (0 0 2) plane of graphite-like tube-wall of the CNTs [21]. In these used catalysts, the Ni–Mo–K components existed mainly in the forms of MoS_2, NiS_x and K–Mo–S with the corresponding XRD features appearing at $2\theta = 13.6^\circ/31.0^\circ$, $35.8^\circ/45.8^\circ/56.2^\circ$ and $19.0^\circ/22.6^\circ/27.2^\circ/32.3^\circ/41.5^\circ$, respectively [11,16,23,24]. Using the

Table 1
Reactivity of syngas conversion to ethanol and higher alcohols over the $Ni_{0.5}Mo_1K_{0.5}$–15%CNTs catalyst and the reference system.[a]

Catalysts	BET[b] ($m^2\ g^{-1}$)	React. condition	X(CO) (%)			Selectivity of hydrogenation products (C%, CO_2-free)							STY ($mg\ h^{-1}\ g^{-1}$)	
			Total	Hydr.	WGS	Total oxy.	MeOH	EtOH	PrOH	BuOH	DME	HCs	Total oxy.	EtOH
$Ni_{0.5}Mo_1K_{0.5}$–15%CNTs	14.2	(i)	13.4	8.4	5.0	67.3	14.5	36.1	11.1	3.2	2.4	32.7	90.3	45.4
		(ii)	13.3	8.4	4.9	64.1	13.8	33.1	11.7	3.8	1.7	35.9	113	55.6
$Ni_{0.5}Mo_1K_{0.5}$	4.1	(i)	9.1	6.2	2.9	62.6	13.9	33.8	9.4	2.7	2.8	37.4	60.9	31.0
		(ii)	9.9	6.4	3.5	57.7	10.2	30.1	12.0	3.9	1.5	42.3	74.7	37.9
$Ni_{0.5}Mo_1K_{0.5}$–15%AC	–	(i)	10.6	7.1	3.5	61.6	14.8	33.1	9.0	2.4	2.3	38.3	69.2	35.0

[a] *Reaction conditions*: (i) 5.0 MPa, 593 K, $V(H_2)/V(CO)/V(N_2)$ = 45/45/10, $GHSV$ = 3000 mL h^{-1} g^{-1} (outlet); (ii) 8.0 MPa, 593 K, $V(H_2)/V(CO)/V(N_2)$ = 45/45/10, $GHSV$ = 4000 mL h^{-1} g^{-1} (outlet); the data were taken 100 h after the reaction started.
[b] In the pre-reduced/sulfurized state.

Scherrer's equation, the average crystallite-size of the three kinds of crystallites, MoS_2, NiS and K–Mo–S, was estimated to be 19.0 nm, 8.4 nm and 7.8 nm for the CNT-containing catalyst, and 32.0 nm, 10.5 nm and 12.3 nm for the CNT-free counterpart. This is in line with the results of the TEM observation (see Fig. 5(b) and (c)). The average crystallite-size of the catalytically active components of the CNT-containing catalyst was comparatively smaller than that of the CNT-free counterpart, indicating the positive role of CNTs in improving the dispersion of particles of MoS_2, NiS_x and K–Mo–S.

3.4.3. Analysis of the used catalysts by XPS

XPS measurements provide information about Ni and Mo species at the quasi-functioning surface of the two tested catalysts of $Ni_{0.5}Mo_1K_{0.5}$–15%CNTs and $Ni_{0.5}Mo_1K_{0.5}$. The measurement results showed that the addition of CNTs to the $Ni_{0.5}Mo_1K_{0.5}$ did not affect the valence state of the Ni^{2+}-species (see Fig. S6). There was little difference between the two tested catalysts in the position and shape of their Ni(2p)-XPS peaks. The XPS peaks of Ni($2p_{3/2}$) and Ni($2p_{1/2}$) observed on the two tested catalysts both exhibited at 856.3 and 873.8 eV (*B.E.*), respectively, with their area-intensity ratio of I(856.3) to I(873.8) being about 2. These values are characteristics of the NiS_x species [25].

Different from the case of Ni(2p)-XPS spectra, certain difference existed between the two used catalysts in the position and shape as well as relative intensity of the peaks associated with the Mo-species. With reference to Ref. [26,27] and assuming E_b(Mo $3d_{3/2}$)–E_b(Mo $3d_{5/2}$) = 3.1 eV and I(Mo $3d_{5/2}$)/I(Mo $3d_{3/2}$) (intensity ratio of the peaks) = 1.5 for each kind of the Mo^{n+} species in the same valence-state, analysis and fitting of these Mo(3d)-XPS spectra were carried out. The results (see Fig. 7) showed that, under the reductive atmosphere containing H_2, CO, etc., most of the Mo^{n+} was reduced to lower valence: the major amount in Mo^{4+}, minor in Mo^{5+}, and few in Mo^{6+}. This was analogous to the case of co-existence of Mo^{4+} (major) with Mo^{5+} (minor) in the related systems [28]. The molar percentage of Mo^{4+}, Mo^{5+} and Mo^{6+} species in the total Mo-amount at the surface of quasi-functioning catalyst was estimated to be 40, 45 and 15 mol% for the $Ni_{0.5}Mo_1K_{0.5}$–15%CNTs, and 19, 33 and 48 mol% for the $Ni_{0.5}Mo_1K_{0.5}$. These results indicate that the surface concentration of Mo^{4+} species of the CNT-containing catalyst was 2.1 times that of the CNT-free counterpart.

Catalysts containing Mo, Group VIII metals, and alkali have been extensively investigated [6–11,29,30]. It is well acknowledged that the activity of the catalysts was mainly associated with the presence of Mo, and that lower oxidation state of Mo (mainly Mo^{4+}) was more active for synthesis of higher alcohols from CO hydrogenation [31]. The higher concentration of surface Mo^{4+}-species, the higher the catalyst activity is. In comparison with the CNT-free host system, higher concentration of surface Mo^{4+}-species of the CNT-containing catalyst was attributed to its higher reducibility, and was also one of the important factors leading to a significant increase of its specific activity for CO hydrogenation.

3.4.4. H_2S/H_2-TPS test of catalysts in oxidation state

H_2S/H_2-TPS of the catalyst provided useful information about the reducibility and sulphidity of catalyst. Fig. 8 shows the H_2S/H_2-TPS profiles taken on the two catalysts in oxidation-state. The H_2S/H_2-reduction/sulfurization of the $Ni_{0.5}Mo_1K_{0.5}$ catalyst (see Fig. 8(b)) started at ca. 453 K and the main TPS-peaks appeared at 586 K, 648 K and 893 K. Previous literatures [32–34] reported that reduction of MoO_3 by H_2S/H_2 to MoO_2 occurred at ca. 650 K, and sulfiding of MoO_2 to MoS_2 occurred at much higher temperatures, and the combination of Ni into MoO_3 might bring about the formation of a Mo–Ni–O composite phase to be easier to be sulfurized, and the sulfiding appeared to be completed at ca. 1100 K in all cases. Therefore, the observed 586-K peak may be ascribed to sulfiding of MoO_3 to MoO_2, and the 648-K peak may be due to sulfiding of MoO_2 to MoS_2, while the higher temperature region (spanning from 693 K to 893 K) likely included the contribution from the sulfiding of bulk compounds (MoO_3, MoO_2), which were difficult to be sulfurized at the lower temperatures. It is worth noting that the doping of CNTs into the $Ni_{0.5}Mo_1K_{0.5}$ resulted in marked down-shifting of the sulfiding peaks (from 586-K, 648-K and 893-K to 468-K, 578-K and 713-K, respectively, see Fig. 8(b) vs. (a)). Conceivably, the lower reduction/sulfurization temperature would be beneficial to inhibiting the aggregation of $Ni_iMo_jK_k$-sulfide crystallites formed by reduction/sulfurization by H_2S/H_2, thus favorable to increasing the exposed area of the $Ni_iMo_jK_k$ components in the pre-reduced/sulfurized state (see Table 1), and subsequently, improving the catalytic activity for higher alcohol synthesis (HAS).

3.4.5. H_2-TPD test of pre-reduced/sulfurized catalysts

The previous literature [35] reported that graphitized carbon black surfaces were capable of rapidly equilibrating H_2/D_2 mixture, and that the active surface area was described in terms of atoms located at edge positions on the graphite basal plane and was determined from the amount of oxygen able to chemisorb at these sites. The previous H_2-TPD investigation by us [36] showed that hydrogen adsorption on the CNTs can occur at ambient temperature and pressures, and that H-species adsorbed on the CNTs may be in two forms: associative (molecular state) and dissociative (atomic state), as evidenced in our Raman spectroscopic study of H_2/CNTs adsorption system [21].

Fig. 9 shows the H_2-TPD profiles of H_2 adsorption on the pre-reduced/sulfurized $Ni_{0.5}Mo_1K_{0.5}$–15%CNTs catalyst and the CNT-free counterpart. Overall, each profile contained a lower-temperature peak (peak I at ca. 363 K) and a higher-temperature peak (peak II at ca. 673 K). The lower-temperature peaks resulted from desorption of the weakly adsorbed H-species, most probably molecularly adsorbed hydrogen, and the higher-temperature peaks were attributed to desorption of the strongly adsorbed H-species, perhaps dissociatively chemisorbed hydrogen [21,36]. It is conceivable that, at the reaction temperatures for HAS (573–613 K for the present work), the concentration of H-adspecies associated with peak-I was very low, and most of H-adspecies at the surface of

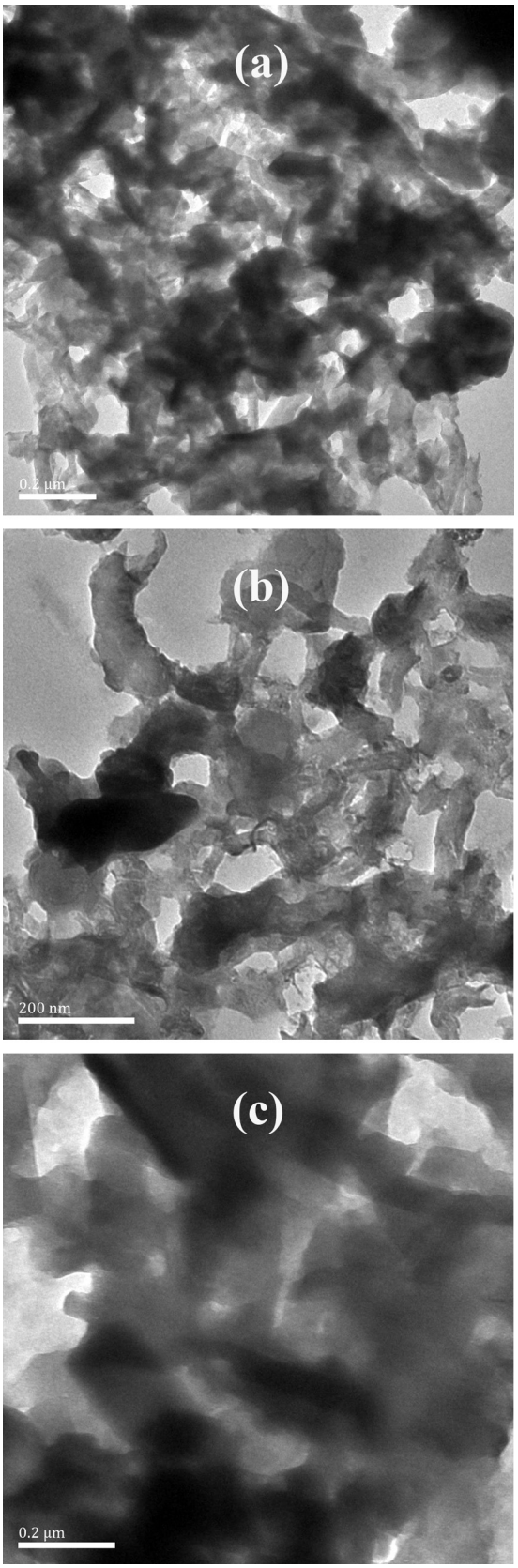

Fig. 5. TEM images of: (a) the pre-reduced/sulfurized $Ni_{0.5}Mo_1K_{0.5}$–15%CNTs; (b) the post-operation $Ni_{0.5}Mo_1K_{0.5}$–15%CNTs; (c) the post-operation $Ni_{0.5}Mo_1K_{0.5}$.

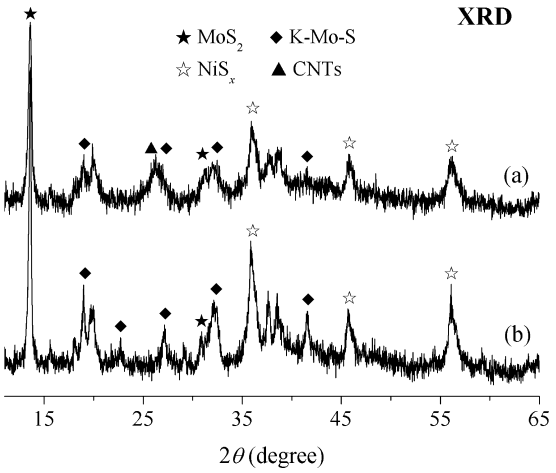

Fig. 6. XRD patterns of the post-operation catalysts: (a) $Ni_{0.5}Mo_1K_{0.5}$–15%CNTs; (b) $Ni_{0.5}Mo_1K_{0.5}$.

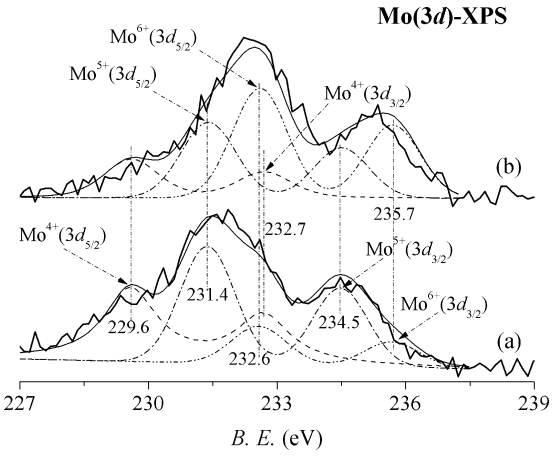

Fig. 7. XPS spectra of Mo(3*d*) of the post-operation catalysts: (a) $Ni_{0.5}Mo_1K_{0.5}$–15%CNTs; (b) $Ni_{0.5}Mo_1K_{0.5}$.

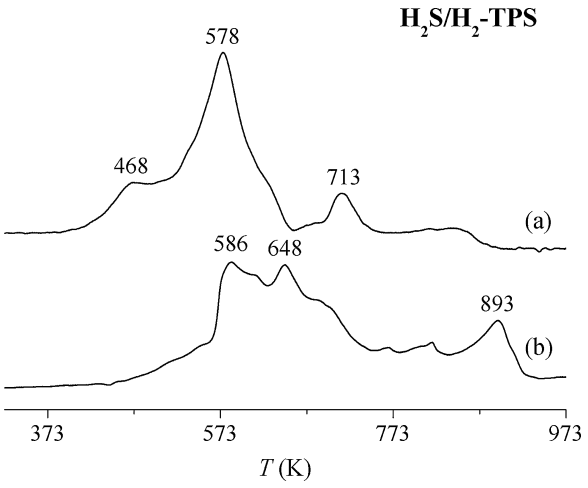

Fig. 8. H_2S/H_2-TPS profiles of the catalyst precursors in oxidation state (a) $Ni_{0.5}Mo_1K_{0.5}$–15%CNTs; (b) $Ni_{0.5}Mo_1K_{0.5}$ (×85%).

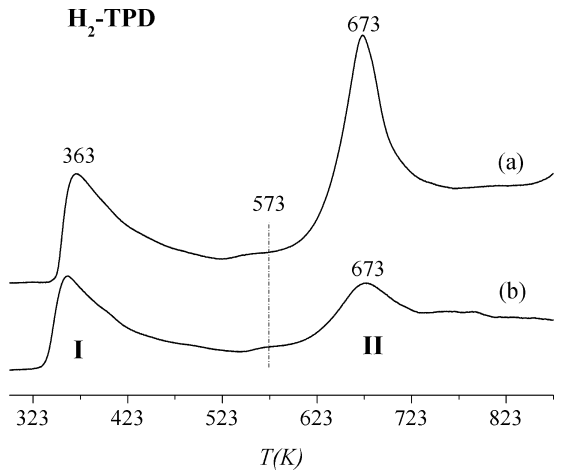

Fig. 9. TPD profiles of H_2 adsorption on the pre-reduced/sulfurized catalysts (a) $Ni_{0.5}Mo_1K_{0.5}$–15%CNTs; (b) $Ni_{0.5}Mo_1K_{0.5}$.

functioning catalysts was those corresponding to peak-II. Hence, it could be inferred that those strongly chemisorbed H-species were closely associated with the reaction activity of CO hydrogenation. The relative area-intensity (I) of the peak-IIs for the two catalysts was estimated to be: $I_{(a)}/I_{(b)} = 100/52$. This was also expected to be the sequence of increase in the stationary-state concentration of H-adspecies at the surface of functioning catalysts, in line with the sequence of the HAS reaction-activity observed on the corresponding catalysts.

H_2-TPD measurement of hydrogen adsorbed was also done on the CNTs with varying grain-sizes: (a) 830–380, (b) 380–180, (c) 180–120, (d) 120–75, (e) 75–38 and (f) ≤38 μm. The result showed that with the grain-size of the CNTs decreasing progressively from 830–380 μm, the amount of desorbed hydrogen increased quickly in the higher grain-size region of (a)–(d), and approached a plateau when the grain-size reached 75–38 μm (e) and below (f) (see Fig. S7). This result implied that the capability of the CNTs to adsorb hydrogen was improved when appropriately reducing its grain size (correspondingly increasing its specific surface area (SSA)). The relative area-intensity (I) of those H_2-TPD profiles in the region of 323–873 K was estimated to be: $I_{(a)}/I_{(b)}/I_{(c)}/I_{(d)}/I_{(e)}/I_{(f)} = 45/50/65/72/95/100$. This was also expected to be the sequence of increase in the stationary-state concentration of H-adspecies at the functioning surface of the corresponding catalysts, in line with the sequence of increase in X(CO-hydr.) observed on the corresponding catalysts (see Fig. 2).

3.5. Nature of promoter action by the CNTs

It is evident that the high reaction activity of hydrogenation–conversion of syngas to C_{1-4}-alcohols, especially ethanol, over the CNT-doped Ni–Mo–K sulfide catalyst is closely related to the peculiar structure and excellent performance for adsorbing/activating H_2 of the CNTs as promoter. It has been well known that the CNTs are a type of two-dimensional nano-carbon, which is close to hollow graphite fiber structurally. In the case of the present work, the CNTs as promoter function through sp^2-C_x at both nanoscale and microscale, rather than individual carbon atoms. The CNTs did not participate in the sulfurized $Ni_iMo_jK_k$ cluster to construct new catalytically active site. Thus, the promoter action by CNTs via their sp^2-C surface to adsorb/activate H_2 may be both short range and medium range (via hydrogen spillover), as supported by the following results in the present work: (1) Addition of a minor amount of the CNTs to the sulfurized $Ni_{0.5}Mo_1K_{0.5}$ catalyst did not cause a marked change in the E_a for the hydrogenation-conversion of syngas (see Fig. S5), implying that the doping of CNTs did not alter the composition and structure of catalytically active site nor the major reaction pathway of CO hydrogenation. (2) Appropriately reducing CNT's grain size could improve the CNT's capability of adsorbing/activating H_2 and, thus, increase rate of hydrogenation–conversion of CO, yet did not influence selectivity of the products (see Figs. 2 and S7).

It follows that the CNTs as promoter function through their adsorbing/activating H_2 to generate a surface micro-environment with higher stationary-state concentration of H-adspecies on the functioning catalyst. This resulted in a dramatic increase, at the surface of the functioning catalyst, of the molar percentage of catalytically active Mo^{4+}/Mo^{5+} species in the total amounts of surface Mo. On the other hand, those active H-species adsorbed at surface of the CNTs could be readily transferred to $Ni_iMo_jK_k$ active sites via the highly conductive CNT-assisted hydrogen spillover. The aforementioned two factors both were conducive to increasing the rate of a series of the surface hydrogenation reactions in the process of syngas hydrogenation-conversion.

4. Concluding remarks

(1) A type of highly efficient Ni–Mo–K sulfide catalyst doped with CNTs for conversion of syngas to ethanol and higher alcohols was developed.
(2) Appropriately reducing CNT's grain-size can improve the promoting effect of CNTs.
(3) CNTs as promoter function through their sp^2-C surface to adsorb and activate hydrogen, so as to generate a surface micro-environment with higher stationary-state concentration of H-adspecies on the functioning catalyst. This resulted in a dramatic increase, at the surface of the functioning catalyst, of the molar percentage of the catalytically active Mo^{4+}/Mo^{5+} species in the total amounts of surface Mo. On the other hand, those active H-species adsorbed at surface of the CNTs could be readily transferred to $Ni_iMo_jK_k$ active sites via the CNT-assisted hydrogen spillover. The aforementioned two factors both were conducive to increasing the rate of hydrogenation conversion of syngas.

Acknowledgements

The work is supported by "973" project (2011CBA00508), NSFC project (20923004), PCSIRT (No. IRT1036) of China.

Appendix A. Supplementary data

Supplementary data associated with this article can be found, in the online version, at http://dx.doi.org/10.1016/j.apcata.2013.08.026.

References

[1] V. Subramani, S.K. Gangwal, Energ. Fuels 22 (2008) 814–839.
[2] G. van der Lee, B. Schuller, H. Post, T.L.F. Favre, V. Ponec, J. Catal. 98 (1986) 522–529.
[3] Y.H. Du, D.A. Chen, K.R. Tsai, Appl. Catal. 35 (1987) 77–92.
[4] H. Ehwald, H. Ewald, D. Gutschick, M. Hermann, H. Miessner, G. Ohlmann, E. Schierhorn, Appl. Catal. 76 (1991) 153–169.
[5] R. Burch, M.J. Hayes, J. Catal. 165 (1997) 249–261.
[6] T. Tatsumi, A. Muramatsu, T. Fukunaga, H. Tominaga, Proc. 9th Intern. Congr. Catal. 2 (1988) 618–625.
[7] J.G. Santiesteban, C.E. Bogdan, R.G. Herman, K. Klier, Proc. 9th Intern. Congr. Catal. 2 (1988) 561–568.
[8] H.-B. Zhang, Y.-Q. Yang, H.-P. Huang, G.-D. Lin, K.R. Tsai, Stud. Surf. Sci. Catal. 75 (1993) 1495–1505.
[9] Z. Li, Y. Fu, J. Bao, M. Jiang, T. Hu, T. Liu, Y-N. Xie, Appl. Catal., A 220 (2001) 21–30.

[10] H. Qi, D. Li, C. Yang, Y. Ma, W. Li, Y. Sun, B. Zhong, Catal. Commun. 4 (2003) 339–342.
[11] D.-B. Li, C. Yang, H.-R. Zhang, W.-H. Li, Y.-H. Sun, B. Zhong, Stud. Surf. Sci. Catal. 147 (2004) 391–396.
[12] J. Iranmahboob, H. Toghiani, D.O. Hill, Appl. Catal. A: Gen. 247 (2003) 207–218.
[13] M. Xiang, D. Li, W. Li, B. Zhong, Y. Sun, Catal. Commun. 8 (2007) 513–518.
[14] J. Bao, Y.L. Fu, G.Z. Bian, Catal. Lett. 121 (2008) 151–157.
[15] V.R. Surisetty, A. Tavasoli, A.K. Dalai, Appl. Catal. A: Gen. 365 (2009) 243–251.
[16] V.R. Surisetty, I. Eswaramoorthi, A.K. Dalai, Fuel 96 (2012) 77–84.
[17] P. Serp, M. Corrias, P. Kalck, Appl. Catal. A: Gen. 253 (2003) 337–358.
[18] H.B. Zhang, G.D. Lin, Y.Z. Yuan, Curr. Topics Catal. 4 (2005) 1–21.
[19] H.B. Zhang, X.L. Liang, X. Dong, H.Y. Li, G.D. Lin, Catal. Surv. Asia 13 (2009) 41–58.
[20] P. Chen, H.B. Zhang, G.D. Lin, Q. Hong, K.R. Tsai, Carbon 35 (1997) 1495–1501.
[21] H.B. Zhang, G.D. Lin, Z.H. Zhou, X. Dong, T. Chen, Carbon 40 (2002) 2429–2436.
[22] J.M. Zhou, H.Y. Li, G.D. Lin, H.B. Zhang, Acta Phys. Chim. Sin. (Chinese) 26 (2010) 3080–3086.
[23] XRD Data Bank Attached to X'Pert PRO X-ray Diffractometer (PANalytical, The Netherlands), 2003.
[24] N. Rueda, R. Bacaud, M. Vrinat, J. Catal. 169 (1997) 404–406.
[25] S. Harris, R.R. Chianelli, J. Catal. 98 (1) (1986) 17–31.
[26] J. Abart, E. Delgado, G. Ertl, H. Jeziorowshi, H. Knözinger, N. Thiele, X.Z. Wang, E. Taglauer, Appl. Catal. 2 (1982) 155–176.
[27] J.F. Moulder, W.F. Stickle, P.E. Sobol, K.D. Bomben, Handbook of X-ray Photoelectron Spectroscopy—A Reference Book of Standard Spectra for Identification and Interpretation of XPS Data, Physical Electronics Inc., Eden Prairie, 1995.
[28] A.M. Venezia, Catal. Today 77 (2003) 359–370.
[29] K. Fujimoto, T. Oba, Appl. Catal. 13 (1985) 289–293.
[30] M. Inoue, T. Miyake, Y. Takegami, T. Inui, Appl. Catal. 29 (1987) 285–294.
[31] A. Muramatsu, T. Tatsumi, H. Tominaga, J. Phys. Chem. 96 (1992) 1334–1340.
[32] P. Arnoldy, J.A.M. van den Heijkant, G.D. de Bok, J.A. Moulijn, J. Catal. 92 (1985) 35–55.
[33] J.F. Liang, R. Guo, X.Y. Yang, J. Mol. Catal. (China) 16 (2002) 15–18.
[34] C.Y. Yang, W.Y. Yang, F.X. Ling, F. Fan, Contemporary Chem. Ind. (China) 39 (2010) 120–122.
[35] Y. Ishikawa, L.G. Austin, D.E. Brown, P.L. Walker Jr., in: P.L. Walker Jr., P.A. Thrower (Eds.), Chemistry and Physics of Carbon, vol. 12, American Carbon Society, Marcel Dekker, New York, 1975, 39-39.
[36] Z.H. Zhou, X.M. Wu, Y. Wang, G.D. Lin, H.B. Zhang, Acta Phys.-Chem. Sin. (Chinese) 18 (2002) 692–698.